ELSEVIER

Journal of Electron Spectroscopy and Related Phenomena 128 (2003) 103–117

JOURNAL OF ELECTRON SPECTROSCOPY and Related Phenomena

www.elsevier.com/locate/elspec

Theoretical molecular Auger spectra with electron population analysis

Masaki Mitani[a], Osamu Takahashi[a], Ko Saito[a,*], Suehiro Iwata[a,b,1]

[a]*Department of Chemistry, Graduate School of Science, Hiroshima University, Higashi-hiroshima, Hiroshima 739-8526, Japan*
[b]*Education and Research Evaluation Division, Faculty of University Evaluation and Research, NIAD, Chiyoda, Tokyo 101-8438, Japan*

Received 27 December 2001; received in revised form 2 May 2002; accepted 8 May 2002

Abstract

An approximation method is proposed to simulate the molecular Auger spectra. Auger transition rates are estimated with atomic populations of valence orbitals on an excited atom by Mulliken and Löwdin population analyses. Normal Auger energies and relative rates for H_2O and NH_3 molecules are evaluated using a full CI wave functions among the valence orbitals constructed from SCF orbitals for the neutral ground state and for the core-hole excited state. Theoretical spectra show fairly good correspondence with the experimental spectra. It is demonstrated that the present approach is applicable for qualitative assignment and analysis of Auger spectra for larger molecules.

Keywords: Core excitation; Auger transition rate; Normal Auger spectrum; Molecular orbital method; Electron population analysis

1. Introduction

Experimental studies for inner-shell excited states by soft X-ray synchrotron radiation have been advanced in recent years. One of the interesting aspects for the core-hole excited (ionic) state of molecules is the site- and state-specific chemical reactions controlled by the excitation (ionization) of a particular core orbital [1–5]. Because the core orbital is well-localized on an atom, its character and energy reflect the chemical environment of the atom in the molecule. With the medium resolution of the photon energy, the selective excitation of an electron in a core orbital at a particular atomic site becomes possible, which may lead to a series of unique decay processes of the atomic site. Recently, the site-specific bond scission by the core excitation was reported for a series of methyl cyanoesters $CH_3OCO(CH_2)_nCN$ ($n = 0$, 1 and 2) in gas phase [6,7] and for poly-methylmethacrylate thin film comprising $-C(CH_3)(COOCH_3)CH_2-$ unit in condensed phase [8,9]. To elucidate the site-specific reaction mechanism, theoretical analyses of experimental observation are crucial. Because these molecules, necessarily in observing the site-specificity, are large polyatomic molecules, a theoretical procedure applicable to large molecules is required.

The processes in a core-excitation reaction involve the photoexcitation of core electron followed by

*Corresponding author. Tel.: +81-824-24-7405; fax: +81-824-24-0726.
E-mail addresses: saito@chem.sci.hiroshima-u.ac.jp (K. Saito), iwata@niad.ac.jp (S. Iwata).
[1]Co-corresponding author. Tel.: +81-3-4212-8050; fax: +81-3-4212-8121.

0368-2048/02/$ – see front matter
PII: S0368-2048(02)00270-0

Auger decay and by rearrangement and dissociation of chemical bonds. We are particularly interested in the bond scission which follows the Auger decay. The fragmentation of molecules after the core excitation has been studied experimentally with multi-coincidence spectroscopies such as photoelectron–photoion coincidence (PEPICO) and Auger electron–photoion coincidence (AEPICO). To theoretically follow the fragmentation processes in detail, the knowledge of the potential energy surfaces with high accuracy for the Auger final states is required; the computations demand extensive cpu time. Consequently, it is obvious that such procedure is practicable only for small molecules such as H_2O [10]. Therefore, alternative much simpler approaches should be developed, and some attempts are now in progress in our group [11,12]. In addition, because the rearrangement and dissociation of chemical bonds take place after the Auger decay except for the processes involving hydrogen atoms, the theoretical construction of Auger spectra is required as the initial step. Thus, the distribution of the Auger final states and transition probabilities has to be calculated.

The theory of molecular Auger spectra [13] has made remarkable progress in the last decade. High levels of calculations taking into account the electron correlation by configuration interaction (CI) [14–19] or by Green's function (GF) [20–22] methods have been performed to construct theoretical Auger spectra in recent years. The energy distribution of Auger final states can be determined by the advanced ab initio procedures on extended configuration spaces. Their effectiveness, however, might be limited to small molecules. The difficulty for large molecules lies not only on the size of electron configuration spaces but also on the number of the final states involved in the Auger transitions. For theoretical evaluation of the Auger transition probability, even for simple molecules except for a few diatomic molecules, the direct application of the first principle approach is still very difficult and rare [13]. So, a fearless approximation method, which is suitable to analyze recent experimental results for large molecules, is to be introduced.

One-center models are an approach to calculate the molecular Auger spectra. In this approach, the molecular Auger rates are approximated using atomic Auger rates, which describe the decay processes of valence atomic orbitals (AOs) within the core-hole atom. But, we have decided not to use them in the present work with a larger basis set. The models are not suitable for the calculations with large basis sets, which are required in our calculations to get the proper energy distribution as demonstrated in text.

In the present article, we calculate the molecular Auger spectra by ab initio molecular orbital (MO) method. An approximation using electron population analysis is introduced to estimate the relative Auger transition rates. The transition rates are written in terms of two-electron integrals among core MO, valence MOs and wave function of Auger electron. We assume the two-electron integral is proportional to the atomic population of valence MOs. This approximation is applied to the normal Auger spectra for H_2O and NH_3 molecules. The purpose of the present paper is to examine the applicability of our approach, and therefore, simple molecules are selected for test case as the first step. The application to larger molecules is reported in separate papers [23].

2. Approximation method

There are two types of inner-shell excitations, after which the Auger decay proceeds; they are called normal and resonant Auger processes. In the normal Auger process an electron from a core orbital is first ionized into continuum states, and then a valence electron fills the vacant core orbital, with the simultaneous ionization from a valence orbital. It is a kind of autoionization. Thus the final states of the normal Auger process are the two valence-hole states. In the resonant Auger process, on the other hand, a core electron is excited to a vacant valence orbital or to a Rydberg orbital, and then the autoionization takes place to the one valence-hole states. In this study, our attention is focused on the theoretical construction of the normal Auger spectra. We assume a two-step model for the Auger process, in which the photoionization and Auger decay are two independent steps. In other words, the interference between two processes is not taken into account. Recently, however, such interference becomes observable with very high resolution excitation condition [24].

In the normal Auger process, the Auger transition rate is written by Fermi's golden rule (Wentzel's ansatz [25]) as follows.

$$T = 2\pi|\langle\Psi_f|\hat{H} - E|\Psi_i\rangle|^2 = 2\pi|t|^2, \quad (1)$$

where Ψ_i and Ψ_f represent the wave functions for the initial state of core-hole cation and for the final state of two valence-hole dication with an ejected Auger electron, respectively, and $\hat{H}$ and E correspond to the Hamiltonian operator and its energy eigenvalue of the initial state. The transition rate T is given by the squared transition amplitude t. If we take a single Slater determinant as Ψ_i and a single configuration state function (CSF), which is a spin- and spatial-symmetry adapted linear combination of Slater determinants, as Ψ_f,

$$\begin{aligned}
&\Psi_{i,c} = \hat{a}_{c,\beta}\Phi_0,\\
&\Psi_{f,vw} = \hat{A}\left\{\sqrt{\frac{1}{2}}\left(\hat{a}_{v,\beta}\hat{a}_{w,\alpha} - \hat{a}_{v,\alpha}\hat{a}_{w,\beta}\right)\Phi_0\phi_k\right\} = \hat{A}({}^1\Phi_{vw}\phi_k),\\
&\Psi_{f,vw} = \hat{A}\left\{\sqrt{\frac{1}{2}}\left(\hat{a}_{v,\beta}\hat{a}_{w,\alpha} + \hat{a}_{v,\alpha}\hat{a}_{w,\beta}\right)\Phi_0\phi_k\right\} = \hat{A}({}^3\Phi_{vw}\phi_k),
\end{aligned} \quad (2)$$

Eq. (1) is reduced to the following for the non-degenerate case [13,26].

$$\begin{aligned}
&{}^1t_{vv} = (cv|kv) \quad (v = w),\\
&{}^1t_{vw} = \sqrt{\frac{1}{2}}\{(cv|kw) + (cw|kv)\} \quad (v \neq w),\\
&{}^3t_{vw} = \sqrt{\frac{3}{2}}\{(cv|kw) - (cw|kv)\} \quad (v \neq w),
\end{aligned} \quad (3)$$

where MOs for core and valence electrons are indicated as c and as v and w, respectively, and k denotes the continuum wave function for an Auger electron. Operators $\hat{a}$ and $\hat{A}$ are annihilation and antisymmetrization operators, and α or β denotes spin of an electron. The superscript specifies the spin multiplicity of the dication. Φ_0 represents closed-shell configuration for the ground state and ${}^{1(3)}\Phi_{vw}$ corresponds to the two-hole singlet (triplet) CSF with holes in the vth and wth MOs for dication. This is the frozen orbital approximation, which means that a common set of MOs is employed for both of the initial and final states. Note that Ψ_f is the doublet state wave function, which is constructed by multiplying the dication wave function and the ejected Auger electron wave function. The term $(ij|kl)$ is a usual two-electron integral for electron repulsion defined by

$$(ij|kl) = \int\int \psi_i(r_1)\psi_j(r_1)\frac{1}{r_{12}}\phi_k(r_2)\psi_l(r_2)\,dr_1\,dr_2. \quad (4)$$

The difficulty in computation of Eq. (3) lies in solving the continuum wave function of the Auger electron. There are a few attempts to obtain the Auger continuum wave function for diatomic molecules. But, as far as our knowledge, no attempts are reported for polyatomic molecules. So a drastic approximation to evaluate the relative Auger transition probability has to be developed to construct the theoretical molecular Auger spectra for polyatomic molecules.

An approximation of one-center models [27,28], employing the matrix element evaluated by the atomic Auger wave function, is applied to a few molecular calculations. The approximation works reasonably well for simple molecules [17–19], but unsatisfactory results are reported for large molecules [29]. The MO-based two-electron integral of Eq. (3) is transformed into AO-based two-electron integrals as

$$\begin{aligned}
(cv|kw) &= \sum_p^{AO}\sum_q^{AO}\sum_r^{AO} C_{pc}C_{qv}C_{rw}(pq|kr)\\
&\approx \sum_q^{AO}\sum_r^{AO} C_{qv}C_{rw}(1sq|kr)\\
&\approx \sum_q^{AO\ on\ C}\sum_r^{AO\ on\ C} C_{qv}C_{rw}(1sq|\kappa r),
\end{aligned} \quad (5)$$

where in the one-center approximation, the summation over AOs q and r included in valence MOs v and w are restricted within the core-hole atom C and the cross-transitions between the other atoms are neglected. In this approximation, it is assumed that core MO c is localized at the core-hole atom C and that it is described by a single 1s AO. The AO-based two-electron integral is calculated using the atomic Auger wave function κ for core-hole atom C in place of the molecular Auger wave function k. A typical example of the one-center model calculations is given in Refs. [30,31]. There, they used the wavefunctions of intermediate neglect of differential

overlap (INDO) approximation for the valence orbitals. The INDO model is based on the minimal basis set without the core orbitals, and therefore, the coefficients of valence AOs C_{qv} and C_{rw} (q, $r=2$s and 2p) can be uniquely defined; only four terms in the sum $\Sigma_q^{\text{on } C}$. But with large basis sets, we cannot uniquely evaluate how much the 2s or 2p AO is contained in the given MOs v and w. It is because the AO is a linear combination of basis sets and their coefficients change in the MO. In other words, there are no unique ways to estimate the weights of AO contributions $|C_{qv}|^2$ and $|C_{rw}|^2$ for q, $r=2$s and 2p in the one-center models. We might be able to estimate the corresponding values by calculating the square of the overlap integrals

$$|\langle \varphi_\mu^{\text{Atom}} | \psi_i^{\text{Molecule}} \rangle|^2 \tag{6}$$

where $\varphi_\mu^{\text{Atom}}$ is the orbitals for the isolated atom determined with the same set of basis functions. This kind of procedure, however, leads another umbiguous approximation. So, we have not decided to adopt the one-center model in the present study. Alternative approach, therefore, should be introduced for our purpose to analyse the Auger decay process in large molecules.

The MO-based two-electron integrals in the formula of the Auger transition rate in Eq. (3) are correlated with the magnitude of overlaps between core and valence MOs, if we neglect the influence by the wave function of the Auger electron. These MO overlaps can be estimated with the electron densities of valence MOs at the core-hole atom, because the core MO is strongly localized on the atom. Therefore, it may be possible to estimate the relative matrix element in Eq. (3) by MO populations

$$\begin{aligned}
{}^1t_{vv} &\approx KP_v(C) \quad (v=w),\\
{}^1t_{vw} &\approx \sqrt{\frac{1}{2}}\,K\{P_v(C)+P_w(C)\} \quad (v\neq w),\\
{}^3t_{vw} &\approx \sqrt{\frac{3}{2}}\,K\{P_v(C)-P_w(C)\} \quad (v\neq w),
\end{aligned} \tag{7}$$

or by density matrix elements

$$\begin{aligned}
{}^1t_{vv} &\approx KD_{cv} \quad (v=w),\\
{}^1t_{vw} &\approx \sqrt{\frac{1}{2}}\,K(D_{cv}+D_{cw}) \quad (v\neq w),\\
{}^3t_{vw} &\approx \sqrt{\frac{3}{2}}\,K(D_{cv}-D_{cw}) \quad (v\neq w),
\end{aligned} \tag{8}$$

$P_v(C)$ and $P_w(C)$ are electron populations of the vth and the wth valence MOs on core-hole atom C, respectively. D_{cv} and D_{cw} are a sum of density matrix elements between core-hole MO and the vth and the wth valence MOs, respectively, defined by

$$D_{ci}=\sum_p^{\text{AO}}\sum_q^{\text{AO}} C_{pc}C_{qi}. \tag{9}$$

Eqs. (7) and (8) mean that MO-based two-electron integrals in Eq. (3) are replaced by $P(C)$ or by D as

$$\begin{aligned}
\frac{(cv|kw)}{P_v(C)} &= \frac{(cw|kv)}{P_w(C)} = K\\
\frac{(cv|kw)}{D_{cv}} &= \frac{(cw|kv)}{D_{cw}} = K.
\end{aligned} \tag{10}$$

In our model, the two-electron integrals involving the core orbital c are assumed to be goverened by the local nature of the valence orbitals v at the core-hole atom C, and are proportional to the partial orbital population $P_v(C)$ at the atom C or the density matrix D_{cv}. Because the continuum function ϕ_k is a fast oscillating function, it is assumed that the overlap density $\phi_k\psi_w$ is less dependent on MO ψ_w. We assume that the proportional constant K is constant for three integrals in Eqs. (7) and (8). In the present work, we fearlessly use a constant K not only for a fixed pair of (v, w) but also for every pair of valence orbitals within a normal Auger spectrum.

3. Computational details

The normal Auger spectra for H_2O and NH_3 molecules are studied to examine the applicability of our model.

Geometrical parameters of molecules are optimized for the neutral ground state by density functional calculations with Becke's three-parameter [32] and Lee–Yang–Parr [33] terms for exchange and correlation functionals, respectively. The molecular structures for core-hole cation and valence-hole dication are fixed to that for the neutral molecule. Because the initial state in the Auger decay process is a core-hole cation, the electron distribution changes from the neutral molecule. To include the orbital relaxation by the core-hole, the MOs should be determined under the electrostatic potential with a core-hole state. The core-hole state is a highly

ionized state, and thus, the usual self-consistent-field (SCF) procedure is not directly applicable, because of the variational collapse to the lower energy state. In this study, the SCF calculation for a core-hole state is performed by using Davidoson's approach [34,35], which avoids the variational collapse. The dynamical damping technique on the density matrix [36] is adopted to improve the convergence. Both SCF MOs determined for the neutral and core-hole molecules are examined in calculating Auger transition rates to see the effects of the core-hole orbital relaxation.

The Mulliken [37] and Löwdin [38] population analyses [39] are used in calculating Auger transition amplitudes given in Eq. (7). In Mulliken partitioning [40], the atomic and overlap populations for atom X and for atoms XY are, respectively, given by

$$P^{\mathrm{Mull}}(X) = \sum_{i}^{\mathrm{MO}} n_i \left(\sum_{p}^{\text{AO on } X} \sum_{q}^{\mathrm{AO}} C_{pi} C_{qi} S_{pq} \right) = \sum_{i}^{\mathrm{MO}} P_i^{\mathrm{Mull}}(X),$$
$$P^{\mathrm{Mull}}(XY) = \sum_{i}^{\mathrm{MO}} n_i \left(\sum_{p}^{\text{AO on } X} \sum_{q}^{\text{AO on } Y} 2 C_{pi} C_{qi} S_{pq} \right) = \sum_{i}^{\mathrm{MO}} P_i^{\mathrm{Mull}}(XY), \tag{11}$$

where n_i is an occupation number of the ith MO, C_{pi} and C_{qi} denote the expansion coefficients for the ith MO and S_{pq} indicates the overlap integral. The populations $P(X)$ and $P(XY)$ can be decomposed into the MO populations of $P_i(X)$ and $P_i(XY)$, respectively, corresponding to the contribution from the ith MO. However, a few difficulties in Mulliken definition has been pointed out [39], in particular for the extensive basis sets with diffuse functions. Therefore, Löwdin analysis, which overcomes a part of the difficulty in Mulliken population [39,41], is also used. Löwdin partitioning is based on the orthogonalized basis functions by symmetric orthogonalization [42], and atomic population is given by

$$P^{\mathrm{Löwd}}(X) = \sum_{i}^{\mathrm{MO}} n_i \left(\sum_{p}^{\text{AO on } X} \sum_{q}^{\mathrm{AO}} \sum_{r}^{\mathrm{AO}} S_{rp}^{1/2} C_{pi} C_{qi} S_{qr}^{1/2} \right) = \sum_{i}^{\mathrm{MO}} P_i^{\mathrm{Löwd}}(X). \tag{12}$$

Because the basis functions are orthogonalized to each other, the overlap populations in Löwdin definition vanish.

The Auger transition rate in Section 2 is given for the single CSF wave function. Because many final states exist within a narrow energy region, the configuration mixing among them becomes significant. Configuration interaction (CI) method should be applied to include the effect. In this work, in the CI expansion all of the valence two-hole configurations are taken into account. The CI wave function of the nth final state is expanded in terms of two-hole CSFs, in which two holes are distributed in the valence occupied MOs. The higher excitation CSFs, such as three-hole one-electron CSF, are not included in the expansion. The Auger intensity for the nth final state is given by the weighted summation of transition rate for each two-hole CSF,

$$\Psi_n = \sum_{v \le w}^{\text{val-occ MO}} C_{n,vw} \hat{A}(\Phi_{vw} \phi_k) = \sum_{v \le w}^{\text{val-occ MO}} C_{n,vw} \Psi_{f,vw},$$
$$t_n = \sum_{v \le w}^{\text{val-occ MO}} C_{n,vw} t_{vw},$$
$$I_n \propto 2\pi |t_n|^2 = 2\pi \left| \sum_{v \le w}^{\text{val-occ MO}} C_{n,vw} t_{vw} \right|^2. \tag{13}$$

The Auger intensity given in Eq. (13) is decomposed into the diagonal and cross terms as

$$I_n \propto 2\pi \sum_{v \le w}^{\text{val-occ MO}} |C_{n,vw}|^2 |t_{vw}|^2 + 2\pi \sum_{v \le w}^{\text{val-occ MO}} \sum_{v' \le w'}^{\text{val-occ MO}} C_{n,vw}^{*} C_{n,v'w'} t_{vw}^{*} t_{v'w'}. \tag{14}$$

In our approach, since the Auger electron wave function is neglected and a two-electron integral is replaced by an electron density, the signs of the CI coefficients in Eq. (14) are not uniquely determined. This means that the cross term of Auger intensity in Eq. (14) may introduce some errors. So, we estimate the intensity by the diagonal term in Eq. (14). The mixing weight among the final state configurations is obtained as the squared coefficient in CI expansion.

The Auger kinetic energy associated with the nth final state is given by the energy difference between the initial cation and the final dication.

To compare with the experimental spectra, the theoretical spectra are constructed by the convolution of the line spectra using Gaussian functions with a fixed value of full width at half maximum (FWHM) over all energy range.

In all calculations, Dunning's correlation-consistent basis sets of cc-pVDZ and cc-pVTZ [43] are used. Geometry optimizations are carried out by the

Table 1
Theoretical and experimental core ionization potentials of H_2O and NH_3 molecules

Molecule	Basis set	Koopmans[a]	ΔSCF[a]	Experiment[a]
H_2O	cc-pVDZ	559.33	541.16	539.93[b]
	cc-pVTZ	559.43	539.44	
NH_3	cc-pVDZ	422.97	407.25	405.55[c]
	cc-pVTZ	422.89	405.61	

[a] Ionization potentials are given in eV.
[b] Experimental value is taken from Ref. [59].
[c] Experimental value is taken from Ref. [51].

Gaussian98 package [44]. The program to calculate the Auger spectra is coded as a part of the MOLYX package [45].

4. Results and discussion

We apply the approximations using the MO population and density matrix to construct the normal Auger spectra of H_2O and NH_3 molecules. Experimental spectra for H_2O [27,46–48] and for NH_3 [49–52] and theoretical spectra for H_2O [27,53–55] and for NH_3 [56–58] have been reported. In this section, we compare our results with those results.

Because the configuration mixing is small for H_2O and NH_3 molecules, the calculated results by full and diagonal expressions in Eq. (14) show the similar spectra. Thus, we give the results using diagonal approximation in this section.

4.1. Core ionized state

At first, we briefly summarize the results for core-ionized H_2O and NH_3 cations before we describe the Auger spectra calculations.

Theoretical and experimental [51,59] core ionization energies IE are given in Table 1. The energies evaluated with the Koopmans theorem [60] and with the ΔSCF calculation are shown. Koopmans IEs overestimate the ionization energies, while the ΔSCF IEs are in good agreement with the experimental values. Thus, Koopmans approach, which is known as fairly good correlation to the IE for valence electrons, is not applicable for the core electrons. The basis set dependence of IE is large in ΔSCF calculation than in Koopmans calculation, and the cc-pVTZ ΔSCF provides a good estimation of the core IE.

Tables 2 and 3 show Mulliken and Löwdin populations obtained from Eqs. (11) and (12) for the neutral and core-hole states of H_2O and NH_3 molecules, respectively. Mulliken and Löwdin analyses give different values for some of the partial atomic populations; for instance $1b_2$ (cc-pVDZ) and $2a_1$ and $1b_2$ (cc-pVTZ) for H_2O, and 1e (cc-pVDZ) and $2a_1$ and 1e (cc-pVTZ) for NH_3. In particular, with a larger basis set, cc-pVTZ, the difference of the two analyses is noticed. The overlap populations of OH and NH bonding MOs ($2a_1$ and $1b_2$ MOs for H_2O, and $2a_1$ and 1e MOs for NH_3) decrease with the core-hole ionization; their bonding nature become slightly weak. We note, as in literature [39,41], that

Table 2
Atomic and overlap populations of the H_2O molecule

Basis set	MO	O(M)[a,b]	O(L)[a,b]	O–H[a]	O*(M)[a,b]	O*(L)[a,b]	O*–H[a]
cc-pVDZ	$1a_1$	2.00	1.99	0.00	1.00	0.99	0.00
	$2a_1$	1.49	1.47	0.31	1.62	1.57	0.26
	$1b_2$	1.17	1.42	0.36	1.49	1.61	0.28
	$3a_1$	1.69	1.80	0.00	1.84	1.89	0.03
	$1b_1$	1.96	1.90	0.04	1.97	1.93	0.03
cc-pVTZ	$1a_1$	2.00	1.97	0.00	1.01	0.98	−0.01
	$2a_1$	1.62	1.26	0.26	1.65	1.33	0.25
	$1b_2$	1.20	1.35	0.37	1.35	1.55	0.32
	$3a_1$	1.70	1.74	−0.01	1.79	1.86	−0.15
	$1b_1$	1.92	1.81	0.07	1.94	1.88	0.05

[a] O and O* represent neutral and core-hole molecules, respectively.
[b] M and L indicate Mulliken and Löwdin populations, respectively.

Table 3
Atomic and overlap populations of NH_3 molecule

Basis set	MO	N(M)[a,b]	N(L)[a,b]	N–H[a]	N*(M)[a,b]	N*(L)[a,b]	N*–H[a]
cc-pVDZ	$1a_1$	2.00	1.98	0.00	1.00	0.99	0.00
	$2a_1$	1.24	1.29	0.27	1.44	1.40	0.23
	1e	2.17	2.66	0.51	2.85	3.04	0.41
	$3a_1$	1.86	1.84	−0.01	1.92	1.89	0.01
cc-pVTZ	$1a_1$	2.00	1.95	0.00	1.03	0.98	−0.03
	$2a_1$	1.43	1.03	0.24	1.50	1.12	0.22
	1e	2.14	2.47	0.52	2.37	2.84	0.47
	$3a_1$	1.86	1.74	0.04	1.86	1.83	−0.11

[a] N and N* represent neutral and core-hole molecules, respectively.
[b] M and L indicate Mulliken and Löwdin populations, respectively.

the Mulliken and Löwdin analyses considerably vary, depending on the basis sets.

4.2. Theoretical Auger spectra with electron density

Four theoretical spectra are shown in Fig. 1 for H_2O and in Fig. 2 for NH_3. The upper two plots (a) and (b) in Figs. 1 and 2 are calculated using the neutral MOs, and the lower two plots (c) and (d) are those using the core-hole MOs. We have noted that the relative intensities slightly vary depending on population analysis; the difference between Mulliken (which is not shown in the figures) and Löwdin results is more significant in cc-pVTZ spectra than in cc-pVDZ spectra, which reflects the difference in the MO populations mentioned in Section 4.1, and the Löwdin population seems to give better results than the Mulliken population. Hereafter, we give the Löwdin spectra only. The relative intensities among the peaks of use of Eq. (7) (the population analysis) and of Eq. (8) (the density matrix) differ from each other. In the latter the lower Auger peaks are more intense than in the former. Because we assume a constant K in Eqs. (7) and (8) for both of the Auger transitions with and without the inner-valence holes, the detailed discussion on the relative intensities for broad energy region is meaningless.

The energies and relative intensities calculated with the cc-pVTZ basis set using the core-hole MOs are given in Tables 4 and 5. Remarkable differences in the upper and lower spectra are noticed. If the core-hole MOs are used in place of the neutral MOs in the CI calculations, the Auger electron energies shift about 15 eV to lower energy, resulting in becoming close to experimental energies without any adjustment. This implies the importance of the core-hole orbital relaxation. The basis set dependence is slightly noticed in the peak energies; compare (a) with (b) and (c) with (d) in Figs. 1 and 2. In particular, spectrum (d) moves to a lower energy from spectrum (c) and becomes more close to the experimental ones, keeping the spectral pattern unchanged.

4.3. Comparison with the experiment

Fig. 3 for H_2O and Fig. 4 for NH_3 compare the experimental Auger spectra [46,51] with the theoretical spectra calculated with the cc-pVTZ basis set. In both figures, the top and bottom plots are the theoretical spectra using neutral and core-hole MOs, respectively, and the middle plot is the experimental spectra, where the observed peaks are labelled as A–X for H_2O and A–G for NH_3, respectively, from high to low energy. Auger kinetic energies of theoretical results are shifted to coincide with the experimental results for the most intense peak. The shifted values are −12.7 eV in the top of Fig. 3, 2.3 eV in the bottom of Fig. 3, −13.8 eV in the top of Fig. 4, and 1.5 eV in the bottom of Fig. 4. The required shift energies are substantially small, if the core-hole MOs are used in the calculations. The number of main peaks in the theoretical and experimental spectra is consistent with each other for both molecules.

The assignments of theoretical spectra based on the core-hole MO calculations are listed in Table 4

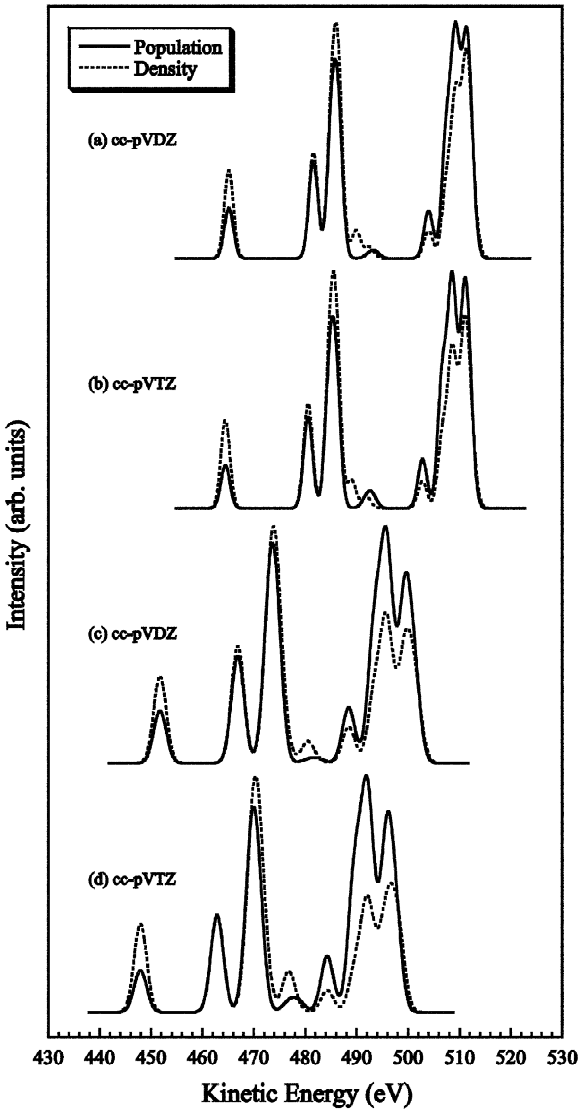

Fig. 1. Theoretical normal Auger spectra for the H_2O molecule calculated by (a) neutral MOs with cc-pVDZ basis set, (b) neutral MOs with cc-pVTZ basis set, (c) core-hole MOs with cc-pVDZ basis set and (d) core-hole MOs with cc-pVTZ basis set. Solid and dotted lines correspond to the resulting spectra by the Löwdin population and density matrix, respectively. FWHM values are (a) 2.5 eV, (b) 2.5 eV, (c) 3.5 eV and (d) 3.5 eV.

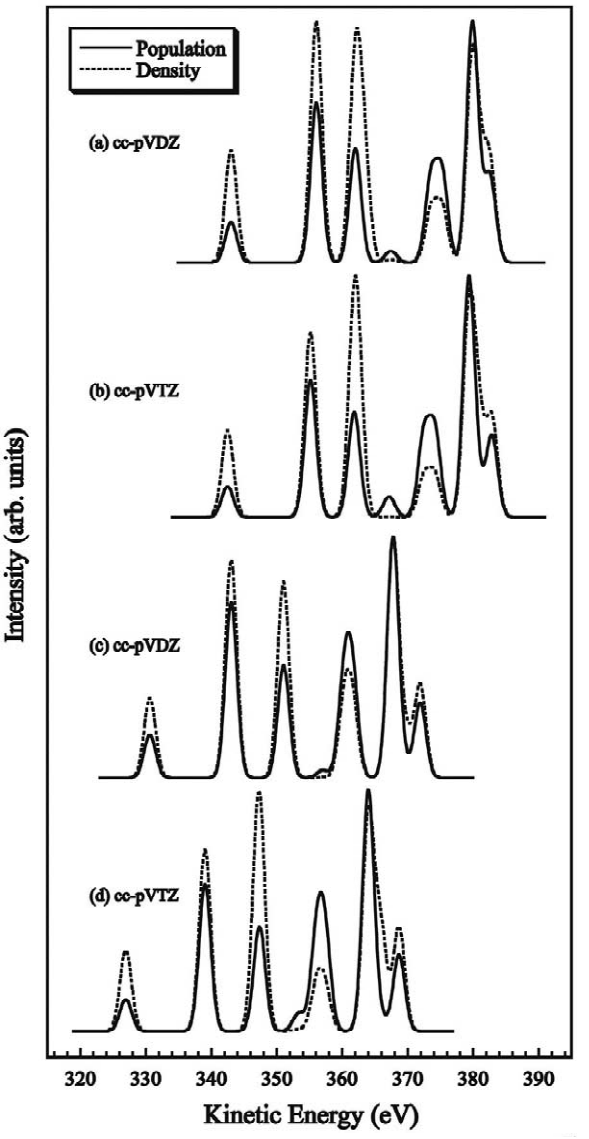

Fig. 2. Theoretical normal Auger spectra for the NH_3 molecule calculated by (a) neutral MOs with cc-pVDZ basis set, (b) neutral MOs with cc-pVTZ basis set, (c) core-hole MOs with cc-pVDZ basis set and (d) core-hole MOs with cc-pVTZ basis set. Solid and dotted lines correspond to resulting spectra by the Löwdin population and density matrix, respectively. FWHM values are (a) 2.5 eV, (b) 2.5 eV, (c) 2.5 eV and (d) 2.5 eV.

for H_2O and in Table 5 for NH_3 together with experimental reports. The almost equivalent assignments are possible using the neutral MO calculations, although the large energy shifts are required. Experimentally, nine (A–X) and seven (A–G) peaks are resolved in H_2O and NH_3 spectra, respectively. The energies for H_2O from three of the independent experimental papers [27,46,48] are almost equal to each other. Peak X in the H_2O spectrum was

Table 4
Assignment of H_2O Auger spectrum using core-hole MO with cc-pVTZ basis set

This work					Peak[e]	Moddeman et al.[f]	Siegbahn et al.[g]	Rye et al.[h]
State[a]	Configuration[b]	Energy[c]	Intensity (P)[d]	Intensity (D)[d]		Energy[c]	Energy[c]	Energy[c]
$^3B_1$	$1.00(3a_1)^{-1}(1b_1)^{-1}$	498.8 (−2.0)	0.00	0.17	A	500.5 (−1.9)	500.8 (−2.2)	
$^1A_1$	$0.96(1b_1)^{-2}$	497.7 (−0.9)	0.50	0.44	B			
$^1B_1$	$0.99(3a_1)^{-1}(1b_1)^{-1}$	495.9 (0.9)	1.00	0.50	B	498.6 (0.0)	498.6 (0.0)	498.6 (0.0)
$^3A_2$	$(1b_2)^{-1}(1b_1)^{-1}$	494.2 (2.6)	0.02	0.15	B,C			
$^1A_1$	$0.93(3a_1)^{-2}$	492.6 (4.2)	0.50	0.13	C			
$^3B_2$	$1.00(1b_2)^{-1}(3a_1)^{-1}$	492.2 (4.6)	0.02	0.00	C			
$^1A_2$	$(1b_2)^{-1}(1b_1)^{-1}$	492.0 (4.8)	0.84	0.52	C	493.8 (4.8)	493.8 (4.8)	493.0 (5.6)
$^1B_2$	$1.00(1b_2)^{-1}(3a_1)^{-1}$	489.7 (7.1)	0.83	0.24	C			
$^1A_1$	$0.97(1b_2)^{-2}$	484.4 (12.4)	0.35	0.14	D	486.8 (11.8)	486.7 (11.9)	486.0 (12.6)
$^3B_1$	$1.00(2a_1)^{-1}(1b_1)^{-1}$	478.8 (18.0)	0.06	0.01	E	482.2 (16.4)	482.1 (16.5)	482.0 (16.6)
$^3A_1$	$(2a_1)^{-1}(3a_1)^{-1}$	476.9 (19.9)	0.06	0.26	E			
$^3B_2$	$1.00(2a_1)^{-1}(1b_2)^{-1}$	472.2 (24.6)	0.01	0.23	F			
$^1B_1$	$0.99(2a_1)^{-1}(1b_1)^{-1}$	470.7 (26.1)	0.74	1.00	F	474.6 (24.0)	475.3 (23.3)	474.2 (24.4)
$^1A_1$	$0.97(2a_1)^{-1}(3a_1)^{-1}$	469.4 (27.4)	0.72	0.57	F		472.4 (26.2)	
$^1B_2$	$1.00(2a_1)^{-1}(1b_2)^{-1}$	463.0 (33.8)	0.59	0.61	G	469.2 (29.4)	467.7 (30.9)	468.0 (30.6)
$^1A_1$	$0.97(2a_1)^{-2}$	448.0 (48.8)	0.26	0.55	H	457.4 (41.2)	457.7 (40.9)	457.0 (41.6)
					X	448.0 (50.6)	450.8 (47.8)	448.0 (50.6)

[a] Spin and spatial symmetries of dication are shown.
[b] Leading hole configurations of final state are listed with configuration weights.
[c] Auger kinetic (relative) energies are given in eV.
[d] Relative intensities obtained by population (P) and density (D) are given in arbitrary units.
[e] Symbols correspond to experimental peaks in Fig. 3.
[f] Experimental values are taken from Ref. [46].
[g] Experimental values are taken from Ref. [27].
[h] Experimental values are taken from Ref. [48].

considered as a satellite peak because of its very weak intensity [27,53]. To confirm the assignment, a CI calculation for the final states including the configurations of $(2a_1)^{-1}(v)^{-1}(w)^{-1}(e)^1$, where v, $w=3a_1$, $1b_1$ and $e=2b_1$, $4a_1$, were carried out and peak X was assigned to the state $(2a_1)^{-1}(3a_1)^{-1}(1b_1)^{-1}(2b_1)^1$ [61]. Three experimental reports for NH_3 [49–51] differ in absolute energy, although they are consistent in relative energy. In the recent experimental [52] and theoretical [62] studies, it was mentioned that the calibration used by Shaw et al. [51] is the most accurate. Concerning peaks C and D in the NH_3 spectrum, two [49,51] or three [50] components were used to fit the experimental data. The higher (360.2 eV [49], 363.0 eV [50] and 359.5 eV [51]) and lower (356.5 eV [49], 360.0 eV [50] and 356.7 eV [51]) components in kinetic energy, which correspond to peaks C and D, were assigned to the ^1E and $^1A_1$ states, respectively, on the basis of the Hartree–Fock (HF) calculation [56], and the $^3A_1$ state was either unassigned [49,51] or assigned to the third component [50]. However, the CI and GF calculations [62] pointed out that the alternate assignment could be more appropriate; the two singlet states ^1E and $^1A_1$ mainly contribute to peak C, and the $^3A_1$ state is responsible for the component at a shoulder D. There is another state $^3A_2$ at the higher side of C in our theoretical calculations, but it has no intensity in both model calculations as seen in Table 5. In Table 5 our modified assignment is given.

Eight peaks A–H in the H_2O spectra are characterized by the nature of the hole MOs in the Auger final state. Peaks A–D are assigned to the states with two holes in the outer valence MOs, $1b_2$, $3a_1$, and $1b_1$ (outer–outer valence). Peaks E–G correspond to the states which have one hole in the $2a_1$ MO and another hole in the other valence MOs (inner–outer valence). Peak H originates from the state having two holes in the $2a_1$ MO (inner–inner valence). The

Table 5
Assignment of NH_3 Auger spectrum using core-hole MO with cc-pVTZ basis set

This work						Shaw et al.[f]		White et al.[g]		Camilloni et al.[h]	
State[a]	Configuration[b]	Energy[c]	Intensity (P)[d]	Intensity (D)[d]	Peak[e]	Energy[c]	Intensity[i]	Energy[c]	Intensity[i]	Energy[c]	Intensity[i]
$^1A_1$	$0.98(3a_1)^{-2}$	368.7 (−4.7)	0.32	0.49	A	370.2 (−4.7)	0.54	371.5 (−4.9)	0.55	374.0 (−4.5)	0.52
^3E	$1.00(1e)^{-1}(3a_1)^{-1}$	365.9 (−1.9)	0.05	0.46	B						
^1E	$1.00(1e)^{-1}(3a_1)^{-1}$	364.0 (0.0)	1.00	1.00	B	365.5 (0.0)	1.00	366.6 (0.0)	0.89	369.5 (0.0)	1.00
$^3A_2$	$(1e)^{-2}$	395.5 (4.6)	0.00	0.00							
^1E	$0.99(1e)^{-2}$	357.4 (6.6)	0.39	0.19	C	359.5 (6.0)	0.68	360.2 (6.4)	1.00	363.0 (6.5)	0.73
$^1A_1$	$0.95(1e)^{-2}$	356.1 (7.9)	0.37	0.20	C						
$^3A_1$	$(2a_1)^{-1}(3a_1)^{-1}$	353.4 (10.6)	0.07	0.01	D	356.7 (8.8)	0.66	356.5 (10.1)	0.14	360.0 (9.5)	0.46
								359.0 (10.5)	0.07		
$^1A_1$	$0.97(2a_1)^{-1}(3a_1)^{-1}$	347.4 (16.6)	0.41	0.85	E	350.9 (14.6)	0.52	352.4 (14.2)	0.45	354.5 (15.0)	0.63
^3E	$1.00(2a_1)^{-1}(1e)^{-1}$	347.0 (17.0)	0.03	0.30	E						
^1E	$0.99(2a_1)^{-1}(1e)^{-1}$	339.1 (24.9)	0.61	0.85	F	343.7 (21.8)	0.66	345.1 (21.5)	0.29	347.4 (22.0)	0.39
$^1A_1$	$0.95(2a_1)^{-2}$	327.0 (37.0)	0.13	0.38	G	334.6 (30.9)	0.36	337.0 (29.6)	0.17	338.8 (30.7)	0.50

[a] Spin and spatial symmetries of dication are shown.
[b] Leading hole configurations of final state are listed with configuration weights.
[c] Auger kinetic (relative) energies are given in eV.
[d] Relative intensities obtained by population (P) and density (D) are given in arbitrary units.
[e] Symbols correspond to experimental peaks in Fig. 4.
[f] Experimental values are taken from Ref. [51].
[g] Experimental values are taken from Ref. [49].
[h] Experimental values are taken from Ref. [50].
[i] Relative intensities are given in arbitrary units.

similar classification of the peaks in the NH_3 spectra is given in Table 5.

The CI calculations with the core-hole relaxation substantially improves the overall agreement of the theoretical spectra with the experimental one. In particular, the calculated relative energies of peaks A–D for H_2O and A–C for NH_3 are in good agreement with the experiments, although the agreement in the relative intensity is not as good as in the energy. The disagreement of the relative intensity for the peaks A–D and E–H in H_2O spectra and for the peaks A–C and D–G in NH_3 spectra is understandable, because we assumed a constant K in Eqs. (7) and (8). Because the final states of peaks E–H for H_2O and D–G for NH_3 involve the inner-valence orbital $2a_1$, the assumption may not hold well. It is also noted that the calculated energies of the final states assigned to peaks E–H for H_2O and D–G for NH_3 overestimate the experimental peak positions substantially higher than those to peaks A–D for H_2O and A–C for NH_3. These final states have one or two holes in the inner-valence orbital. It is known that in the ordinal photoelectron spectrum (or in the corresponding $e-2e$ momentum transfer spectrum) the ionic states of the inner-valence orbitals are strongly mixed with the two-hole one-particle states, resulting in a few shake-up states. Similarly in the Auger final states, it is expected that the configuration mixing among three-hole one-particle states and the inner-valence hole states is strong [61–63]. The neglect of three-hole one-particle states results in the overestimation of the energy. The broad background in the experimental spectrum might be analyzed in terms of these three-hole one-particle states, whose state density is large to form the quasi continuum background.

4.4. Comparison with the previous calculation

Several theoretical studies have been reported for the normal Auger spectra for H_2O [27,53–55] and NH_3 [56–58] at the various levels of approximation. We here briefly mention their approach, and the details of computation are described in the references. The following procedures were applied to (i) Auger intensity and (ii) Auger energy calculations.

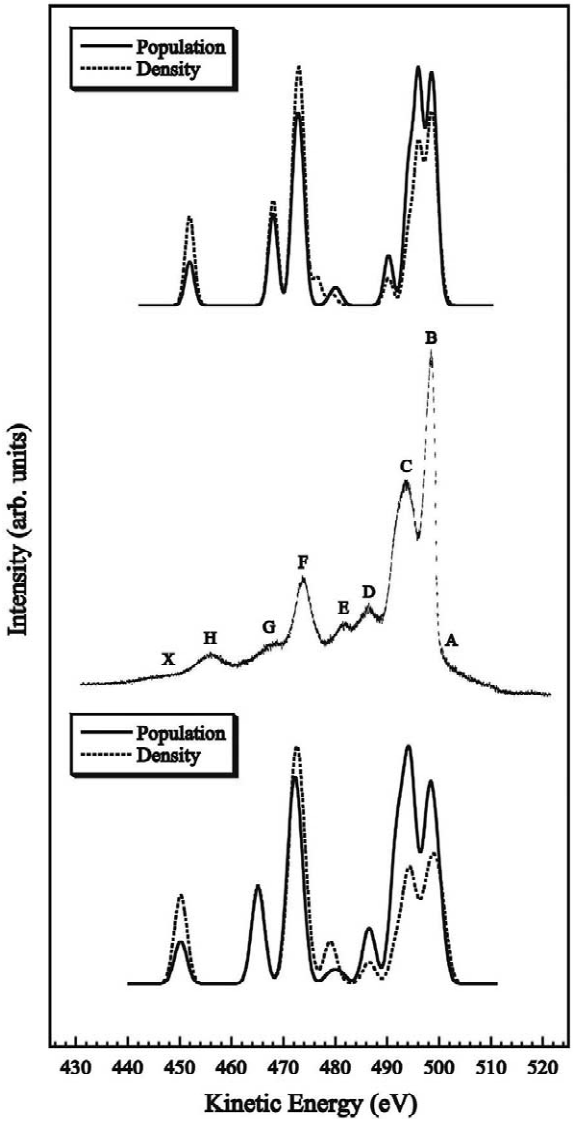

Fig. 3. Theoretical and experimental normal Auger spectra for H_2O molecule. Top and bottom plots are cc-pVTZ results using neutral and core-hole MOs, respectively. Solid and dotted lines correspond to resulting spectra by the Löwdin population and density matrix, respectively. Experimental spectrum given by Moddeman et al. [46] is shown as the middle plot. Symbols A–X are added by the present authors for convenience. Auger kinetic energy for theoretical spectra is shifted to coincide with the experimental spectra (see text for shifted values). Theoretical and experimental data for energy and intensity are summarized in Table 4.

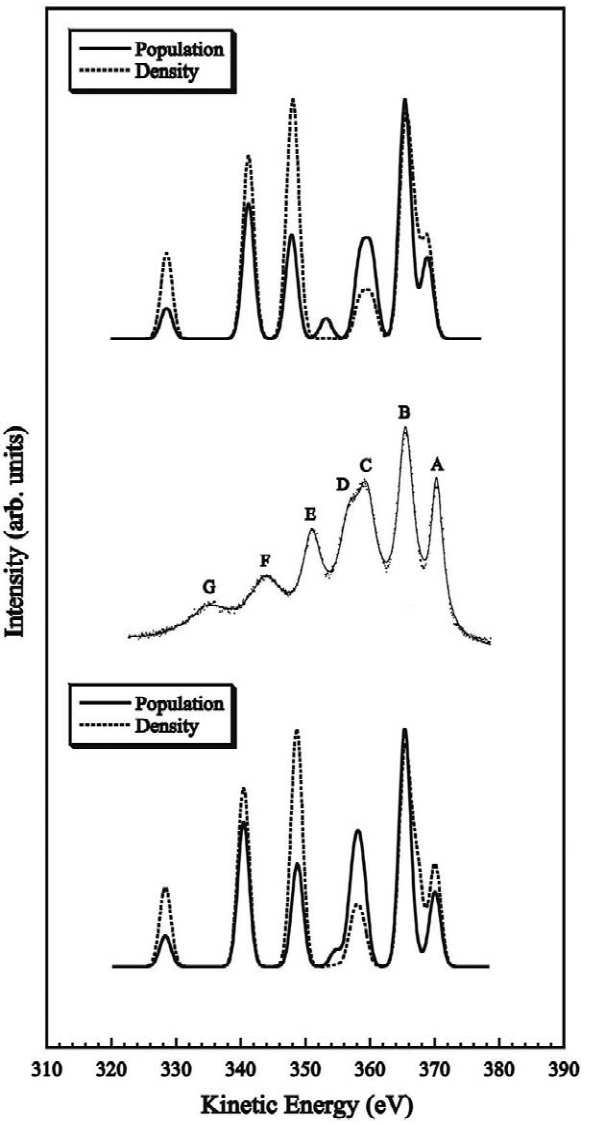

Fig. 4. Theoretical and experimental normal Auger spectra for NH_3 molecule. Top and bottom plots are cc-pVTZ results using neutral and core-hole MOs, respectively. Solid and dotted lines correspond to resulting spectra by the Löwdin population and density matrix, respectively. Experimental spectrum given by Shaw et al. [51] is shown as the middle plot. Symbols A–G are added by the present authors for convenience. Auger kinetic energy for theoretical spectra is shifted to coincide with the experimental spectra (see text for shifted values). Theoretical and experimental data for energy and intensity are summarized in Table 5.

Table 6
Theoretical calculations of the Auger spectrum of H_2O molecule

State[a]	Configuration[b]	Siegbahn et al.[c]		Carravetta et al.[d]		Liegener et al.[e]	
		Energy[f]	Intensity[g]	Energy[f]	Intensity[g]	Energy[f]	Intensity[g]
$^3B_1$	$(3a_1)^{-1}(1b_1)^{-1}$	502.6 (−2.5)	0.02	500.7 (−2.0)	0.02	499.4 (−1.3)	0.04
$^1A_1$	$(1b_1)^{-2}$	500.8 (−0.6)	1.00	499.4 (−0.7)	0.98	498.7 (−0.7)	0.81
$^1B_1$	$(3a_1)^{-1}(1b_1)^{-1}$	499.6 (0.6)	0.99	498.0 (0.7)	1.00	497.4 (0.7)	1.00
$^3A_2$	$(1b_2)^{-1}(1b_1)^{-1}$	497.7 (2.4)	0.00	496.4 (2.3)	0.00		
$^1A_1$	$(3a_1)^{-2}$	496.4 (3.8)	0.71	494.6 (4.1)	0.67	495.2 (2.9)	0.69
$^3B_2$	$(1b_2)^{-1}(3a_1)^{-1}$	496.4 (3.8)	0.01	494.4 (4.3)	0.02	493.6 (4.4)	0.02
$^1A_2$	$(1b_2)^{-1}(1b_1)^{-1}$	495.7 (4.5)	0.74	494.4 (4.3)	0.90	493.8 (4.3)	0.51
$^1B_2$	$(1b_2)^{-1}(3a_1)^{-1}$	493.8 (6.4)	0.58	492.1 (6.5)	0.94	491.8 (6.2)	0.43
$^1A_1$	$(1b_2)^{-2}$	488.3 (11.9)	0.34	487.4 (11.3)	0.59	486.8 (11.2)	0.17
$^3B_1$	$(2a_1)^{-1}(1b_1)^{-1}$	482.1 (18.0)	0.14	482.1 (16.5)	0.27	481.3 (16.7)	0.14
$^3A_1$	$(2a_1)^{-1}(3a_1)^{-1}$	480.7 (19.5)	0.11	483.5 (15.2)	0.28	479.9 (18.1)	0.11
$^3B_2$	$(2a_1)^{-1}(1b_2)^{-1}$	475.8 (24.3)	0.08	476.6 (22.1)	0.21	475.6 (22.4)	0.06
$^1B_1$	$(2a_1)^{-1}(1b_1)^{-1}$	474.0 (26.2)	0.55	475.7 (23.0)	0.57	475.9 (22.1)	0.56
$^1A_1$	$(2a_1)^{-1}(3a_1)^{-1}$	473.5 (26.7)	0.48	472.1 (26.6)	0.64	474.6 (23.4)	0.75
$^1B_2$	$(2a_1)^{-1}(1b_2)^{-1}$	467.3 (32.9)	0.32	467.6 (31.1)	0.44	469.1 (28.9)	0.23
$^1A_1$	$(2a_1)^{-2}$	451.5 (48.7)	0.48	458.3 (40.4)	0.60	456.3 (41.7)	0.48

[a] Spin and spatial symmetries of dication are shown.
[b] Hole configurations of final state are listed.
[c] Theoretical values are taken from Refs. [27,53].
[d] Theoretical values are taken from Ref. [54].
[e] Theoretical values are taken from Ref. [55].
[f] Auger kinetic (relative) energies are given in eV.
[g] Relative intensities are given in arbitrary units.

Table 7
Theoretical calculations of Auger spectrum of NH_3 molecule

State[a]	Configuration[b]	Økland et al.[c]		Jennison[d]		Larkins et al.[e]	
		Energy[f]	Intensity[g]	Energy[f]	Intensity[g]	Energy[f]	Intensity[g]
$^1A_1$	$(3a_1)^{-2}$	373.7 (−4.1)	0.50	366.3 (−2.0)	0.53	363.5 (−1.0)	0.64
^3E	$(1e)^{-1}(3a_1)^{-1}$	371.5 (−1.9)	0.02	365.7 (−1.4)	0.01	363.8 (−1.3)	0.03
^1E	$(1e)^{-1}(3a_1)^{-1}$	369.6 (0.0)	1.00	364.3 (0.0)	1.00	362.5 (0.0)	1.00
$^3A_2$	$(1e)^{-2}$	365.4 (4.2)	0.02	361.7 (2.6)	0.00	360.6 (1.9)	0.00
^1E	$(1e)^{-2}$	363.1 (6.5)	1.00	359.5 (4.8)	0.63	359.4 (3.1)	0.59
$^1A_1$	$(1e)^{-2}$	360.8 (8.8)	0.27	357.3 (7.0)	0.28	358.1 (4.4)	0.18
$^3A_1$	$(2a_1)^{-1}(3a_1)^{-1}$	358.8 (10.8)	0.06	353.9 (10.4)	0.12	352.3 (10.2)	0.12
$^1A_1$	$(2a_1)^{-1}(3a_1)^{-1}$	352.9 (16.7)	0.14	349.0 (15.3)	0.44	349.3 (13.2)	0.47
^3E	$(2a_1)^{-1}(1e)^{-1}$	352.8 (16.8)	0.12	349.9 (14.4)	0.16	348.8 (13.7)	0.14
^1E	$(2a_1)^{-1}(1e)^{-1}$	345.1 (24.5)	0.29	343.1 (21.2)	0.52	345.4 (17.1)	0.42
$^1A_1$	$(2a_1)^{-2}$	333.9 (35.7)	0.17	332.7 (31.6)	0.48	334.6 (27.9)	0.32

[a] Spin and spatial symmetries of dication are shown.
[b] Hole configurations of final state are listed.
[c] Theoretical values are taken from Ref. [56].
[d] Theoretical values are taken from Ref. [57].
[e] Theoretical values are taken from Ref. [58].
[f] Auger kinetic (relative) energies are given in eV.
[g] Relative intensities are given in arbitrary units.

Siegbahn et al. [27] and also Ågren et al. [53] used (i) atomic matrix element and (ii) restricted open-shell HF (ROHF) and CI methods. Carravetta et al. [54] applied (i) Stieltjes imaging and (ii) multi-configuration SCF (MCSCF) and CI methods. Liegener et al. [55] combined (i) atomic matrix element with (ii) GF method. Økland et al. [56] combined (i) Ne atom intensity with (ii) ROHF method. Jennison [57] used (i) atomic matrix ele-

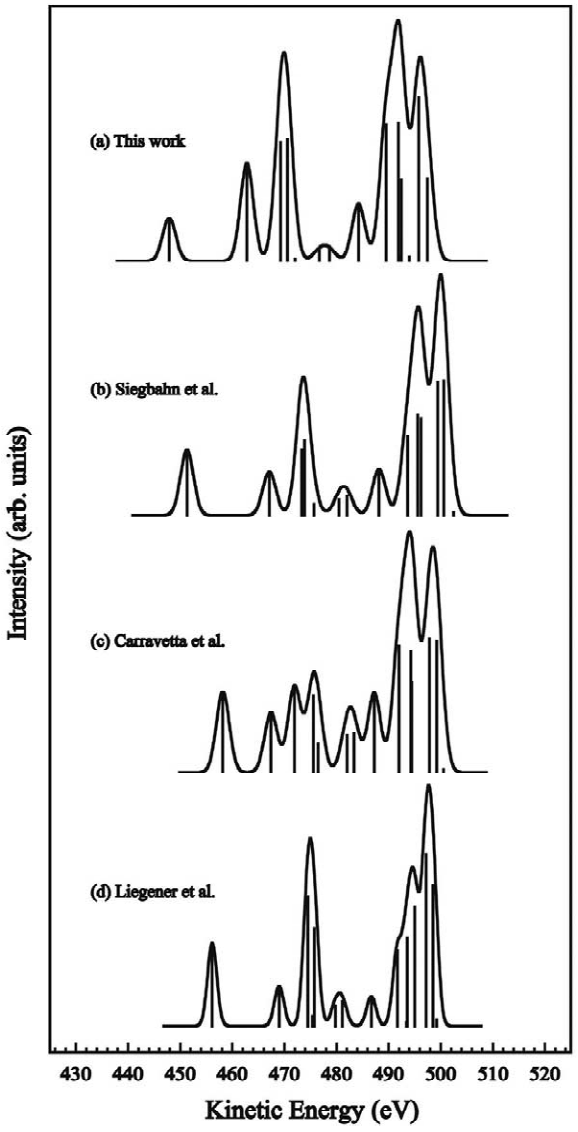

Fig. 5. Theoretical normal Auger spectra for the H_2O molecule reported by (a) this work, (b) Siegbahn et al. [27,53], (c) Carravetta et al. [54] and (d) Liegener et al. [55]. Plot by this work is obtained from the Löwdin population using core-hole MOs with cc-pVTZ basis set. Theoretical data for energy and intensity are summarized in Table 6. FWHM values are (a) 3.5 eV, (b) 3.5 eV, (c) 3.5 eV and (d) 2.5 eV.

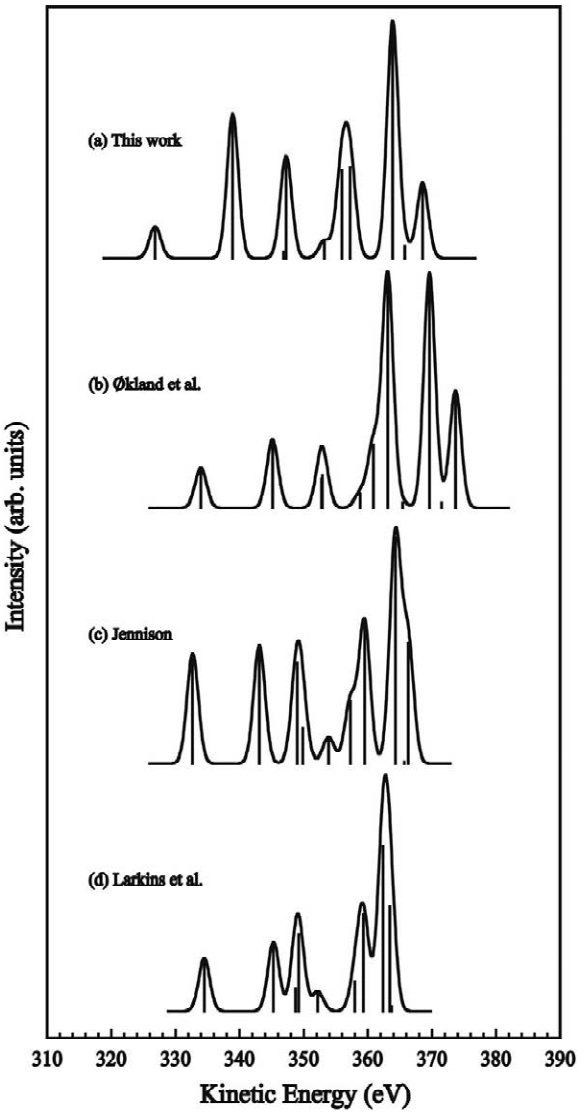

Fig. 6. Theoretical normal Auger spectra for the NH_3 molecule reported by (a) this work, (b) Økland et al. [56], (c) Jennison [57] and (d) Larkins et al. [58]. Plot by this work is obtained from the Löwdin population using core-hole MOs with cc-pVTZ basis set. Theoretical data for energy and intensity are summarized in Table 7. FWHM values are (a) 2.5 eV, (b) 2.5 eV, (c) 2.5 eV and (d) 2.5 eV.

ment and (ii) ROHF method. Larkins et al. [58] used (ii) semiempirical HF wave function of INDO approximation with (i) atomic matrix element.

In order to compare our results with the results mentioned above, we performed Gaussian convolution using the data reported in the references. The energies and intensities for H_2O and NH_3 are summarized in Tables 6 and 7, respectively, and the Auger spectra for H_2O and NH_3 are given in Figs. 5 and 6, respectively. We show our results obtained form the Löwdin population in Figs. 5 and 6.

All of the theoretical H_2O spectra in Fig. 5 well reproduce the characteristic features of the experimental spectrum. The best correspondence to the experiment seems to be the spectrum (b) by Siegbahn et al. [27,53], although the most accurate approximation is for the spectrum (c) by Carravetta et al. [54]. The Stieltjes imaging slightly overestimate the relative intensities for triplet components included in the peaks E and F than the others. Our result (a) show a similar shape of spectrum with spectrum (b) of Siegbahn et al. On the other hand, the theoretical spectra for NH_3 in Fig. 6 differ to each other. Especially, the energy distribution by INDO calculation (d) is unsatisfactory. Also, the shifts for peaks C and D from the main peak are incorrect in (b) and (c), because the electron correlation is not taken into account by the SCF level of approximation as denoted in Section 4.3. Our CI spectrum (a) improves the relative energy substantially.

5. Conclusions

In this work, we construct the normal Auger spectra of H_2O and NH_3, using the simple model calculations for the transition probabilities with limited CI calculations. Theoretical spectra successfully reproduce the main feature of the experimental spectra when the core-hole MOs with the cc-pVTZ basis set are used in the calculations. The cc-pVDZ basis set might also be able to be used with a slight adjustment in the energy scale.

We have tested our fearless approximation models to two simple molecules. Judging from the present results, we might be able to expect that the models might be useful in analysing the Auger spectra of larger molecules. We have already applied to the other molecules and will report the results elsewhere. In particular, the calculations for H_2CO, HNH_2CO, HCH_3CO and $(CH_3)_2CO$ molecules is interesting [23], because it was reported that the theoretical spectra employing the atomic matrix element are not sufficient in early work [29]. The study for resonant Auger spectra by this method is also now in progress.

Finally, we should mention a few restrictions of our model; (1) the configuration space of CI wave functions is limited within the valence two-hole configuration and (2) Auger continuum wave function is completely neglected. As for (1), it is not so difficult to extend the calculations by including the higher excited configuration of three-hole one-particle states with an appropriate set of one-particle orbitals, and the satellite peaks may be obtained. On the other hand, concerning (2), it is difficult to solve Auger continuum directly for polyatomic molecules, thus, a practical approximation method for large molecules is needed. This is a challenging subject, which should be developed in the future.

Acknowledgements

This study was supported by a Grant-in-Aid on Research for the Future ‘Photoscience’ (JSPS-RFTF-98P01202) from Japan Society for the Promotion of Science.

References

[1] W. Eberhardt, T.K. Sham, R. Carr, S. Krummacher, M. Strongin, S.L. Weng, D. Wesner, Phys. Rev. Lett. 40 (1983) 1038.
[2] D.M. Hanson, Adv. Chem. Phys. 77 (1990) 1.
[3] S. Nagaoka, K. Mase, I. Koyano, Nucl. Trends Chem. Phys. 6 (1997) 1.
[4] T. Sekitani, E. Ikenaga, K. Fujii, K. Mase, N. Ueno, K. Tanaka, J. Electron Spectrosc. Relat. Phenom. 101–103 (1999) 135.
[5] K. Tanaka, E.O. Sako, E. Ikenaga, K. Isari, S.A. Sardar, S. Wada, T. Sekitani, K. Mase, N. Ueno, J. Electron Spectrosc. Relat. Phenom. 119 (2001) 255.
[6] T. Ibuki, K. Okada, K. Saito, T. Gejo, J. Electron Spectrosc. Relat. Phenom. 107 (2000) 39.
[7] K. Okada et al., private communication.

[8] E. Ikenaga, K. Kudara, K. Kusaba, K. Isari, S.A. Sardar, S. Wada, K. Mase, T. Sekitani, K. Tanaka, J. Electron Spectrosc. Relat. Phenom. 114–116 (2001) 585.
[9] E. Ikenaga, K. Isari, K. Kudara, Y. Yasui, S.A. Sardar, S. Wada, T. Sekitani, K. Tanaka, K. Mase, S. Tanaka, J. Chem. Phys. 114 (2001) 2751.
[10] K. Nobusada, K. Tanaka, J. Chem. Phys. 112 (2000) 7437.
[11] E.O. Sako, Y. Kanameda, E. Ikenaga, M. Mitani, O. Takahashi, K. Saito, S. Iwata, S. Wada, T. Sekitani, K. Tanaka, J. Electron Spectrosc. Relat. Phenom. 114–116 (2001) 591.
[12] O. Takahashi, M. Mitani, M. Joyabu, K. Saito, S. Iwata, J. Electron Spectrosc. Relat. Phenom. 120 (2001) 137.
[13] H. Ågren, A. Cesar, C.-M. Liegener, Adv. Quantum Chem. 23 (1992) 1, and references are therein.
[14] B. Scimmelpfenning, B.M. Nestmann, S.D. Peyerimhoff, J. Electron Spectrosc. Relat. Phenom. 74 (1995) 173.
[15] B. Scimmelpfenning, S.D. Peyerimhoff, Chem. Phys. Lett. 253 (1996) 377.
[16] S.K. Botting, R.R. Lucchese, Phys. Rev. A 56 (1997) 3666.
[17] R. Fink, J. Electron Spectrosc. Relat. Phenom. 76 (1995) 295.
[18] R. Fink, J. Chem. Phys. 106 (1997) 4038.
[19] R.F. Fink, S.L. Sorensen, A. Naves de Brito, A. Ausmees, S. Svensson, J. Chem. Phys. 112 (2000) 6666.
[20] F. Tarantelli, A. Sgamellotti, L.S. Cederbaum, J. Electron Spectrosc. Relat. Phenom. 68 (1994) 297.
[21] D. Minelli, F. Tarantelli, A. Sgamellotti, L.S. Cederbaum, J. Electron Spectrosc. Relat. Phenom. 74 (1995) 1.
[22] F. Tarantelli, L.S. Cederbaum, A. Sgamellotti, J. Electron Spectrosc. Relat. Phenom. 76 (1995) 47.
[23] M. Mitani, O.Takahashi, K. Saito, S. Iwata, in preparation.
[24] T. Ibuki, K. Kamimori, K. Okada, J. Sasaki, S. Nagaoka, I.H. Suzuki, Y. Shimizu, N. Saito, Y. Tamenori, H. Ohashi, A. Hiraya, H. Yoshida, 17th Symposium on Chemical Kinetics and Dynamics, Fukuoka, Japan, May, 2001, Book of Abstracts, 3P16.
[25] G. Wentzel, Z. Phys. 43 (1927) 521.
[26] R. Manne, H. Ågren, Chem. Phys. 93 (1985) 201.
[27] H. Siegbahn, L. Asplund, P. Kelfve, Chem. Phys. Lett. 35 (1975) 330.
[28] D.E. Ramaker, J.S. Murday, N.H. Turner, G. Moore, M.G. Lagally, J. Houston, Phys. Rev. B 19 (1979) 5375.
[29] N. Correia, A. Naves de Brito, M.P. Keane, L. Karlsson, S. Svensson, C.-M. Liegener, A. Cesar, H. Ågren, J. Chem. Phys. 95 (1991) 5187.
[30] M.H. Chen, F.P. Larkins, B. Crasemann, At. Nucl. Data Tables 45 (1990) 1.
[31] E.Z. Chelkowska, F.P. Larkins, At. Nucl. Data Tables 49 (1991) 121.
[32] A.D. Becke, J. Chem. Phys. 98 (1993) 5648.
[33] C. Lee, W. Yang, R.G. Parr, Phys. Rev. B 37 (1988) 785.
[34] H.-L. Hsu, E.R. Davidson, R.M. Pitzer, J. Chem. Phys. 65 (1976) 609.
[35] E.R. Davidson, L.Z. Stenkamp, Int. J Quantum Chem. Symp. 10 (1976) 21.
[36] M.C. Zerner, M. Hehenberger, Chem. Phys. Lett. 62 (1979) 550.
[37] R.S. Mulliken, J. Chem. Phys. 36 (1962) 3428.
[38] P.-O. Löwdin, Adv. Quantum Chem. 5 (1970) 185.
[39] F. Jensen, Introduction to Computational Chemistry, Wiley, Chichester, 1999, Chapter 9.
[40] R.S. Mulliken, J. Chem. Phys. 23 (1953) 1833, 1841.
[41] T. Nagata, O. Takahashi, K. Saito, S. Iwata, J. Chem. Phys. 115 (2001) 2553.
[42] P.-O. Löwdin, J. Chem. Phys. 18 (1950) 365.
[43] T.H. Dunning Jr, J. Chem. Phys. 90 (1989) 1007.
[44] M.J. Frisch, G.W. Trucks, H.B. Schlegel, G.E. Scuseria, M.A. Robb, J.R. Cheeseman, V.G. Zakrzewski, J.A. Montgomery Jr, R.E. Stratmann, J.C. Burant, S. Dapprich, J.M. Millam, A.D. Daniels, K.N. Kudin, M.C. Strain, O. Farkas, J. Tomasi, V. Barone, M. Cossi, R. Cammi, B. Mennucci, C. Pomelli, C. Adamo, S. Clifford, J. Ochterski, G.A. Petersson, P.Y. Ayala, Q. Cui, K. Morokuma, D.K. Malick, A.D. Rabuck, K. Raghavachari, J.B. Foresman, J. Cioslowski, J.V. Ortiz, B.B. Stefanov, G. Liu, A. Liashenko, P. Piskorz, I. Komaromi, R. Gomperts, R.L. Martin, D.J. Fox, T. Keith, M.A. Al-Laham, C.Y. Peng, A. Nanayakkara, C. Gonzalez, M. Challacombe, P.M.W. Gill, B. Johnson, W. Chen, M.W. Wong, J.L. Andres, C. Gonzalez, M. Head-Gordon, E.S. Replogle, J.A. Pople, Gaussian 98, Gaussian, Inc., Pittsburgh PA, 1998, Revision A.5.
[45] S. Iwata, http://hera.ims.ac.jp/ and http://home.hiroshima-u.ac.jp/core/.
[46] W.E. Moddeman, T.A. Carlson, M.O. Krause, B.P. Pullen, W.E. Bull, G.K. Schweitzer, J. Chem. Phys. 55 (1971) 2317.
[47] J.A. Connor, I.H. Hillier, J. Kendrick, M. Barber, A. Barrie, J. Chem. Phys. 64 (1976) 3325.
[48] R.R. Rye, T.E. Madey, J.E. Houston, P.H. Holloway, J. Chem. Phys. 69 (1978) 1504.
[49] J.M. White, R.R. Rye, J.E. Houston, Chem. Phys. Lett. 46 (1977) 146.
[50] R. Camilloni, G. Stefani, A. Giardini-Guidoni, Chem. Phys. Lett. 50 (1977) 213.
[51] R.W. Shaw Jr, J.S. Jen, T.D. Thomas, J. Electron Spectrosc. Relat. Phenom. 11 (1977) 91.
[52] C.I. Ma, D.M. Hanson, K. Lee, R.G. Hayes, J. Electron Spectrosc. Relat. Phenom. 75 (1995) 83.
[53] H. Ågren, S. Svensson, U.I. Wahlgren, Chem. Phys. Lett. 35 (1975) 336.
[54] V. Carravetta, H. Ågren, Phys. Rev. A 35 (1987) 1022.
[55] C.-M. Liegener, R. Chen, J. Chem. Phys. 88 (1988) 2618.
[56] M.T. Økland, K. Fægri Jr, R. Manne, Chem. Phys. Lett. 40 (1976) 185.
[57] D.R. Jennison, Phys. Rev. A 23 (1981) 1215.
[58] F.P. Larkins, L.C. Tulea, E.Z. Chelkowska, Aust. J. Phys. 43 (1990) 625.
[59] K. Siegbahn, J. Electron Spectrosc. Relat. Phenom. 5 (1974) 3.
[60] T.A. Koopmans, Physica 1 (1933) 104.
[61] H. Ågren, H. Siegbahn, Chem. Phys. Lett. 69 (1980) 424.
[62] F. Tarantelli, A. Tarantelli, A. Sgamellotti, J. Schirmer, L.S. Cederbaum, Chem. Phys. Lett. 117 (1985) 577.
[63] F. Tarantelli, A. Tarantelli, A. Sgamellotti, J. Schirmer, L.S. Cederbaum, J. Chem. Phys. 83 (1985) 4683.